ASTER/TIR onboard calibration status and user-based recalibration

Hideyuki Tonooka*[a], Fumihiro Sakuma[b], Masahiko Kudoh[c], Koji Iwafune[d]

[a]Ibaraki Univ., 4-12-1 Nakanarusawa, Hitachi, Ibaraki, Japan 316-8511;
[b]National Metrology Inst. of Japan/AIST, 1-1-1 Umezono, Tsukuba, Ibaraki, Japan 305-8563;
[c]Japan Resources Observation System Org., 2-20-1 Hatchobori, Chuo, Tokyo, Japan 104-0032;
[d]Fujitsu Ltd., 4-1-1 Kamikodanaka, Nakahara, Kawasaki, Kanagawa, Japan 211-8588

ABSTRACT

Advanced Spaceborne Thermal Emission and Reflection Radiometer (ASTER), one of five sensors on Terra, has five bands (10 to 14) in the thermal infrared (TIR) region. These TIR bands are radiometrically calibrated by one onboard blackbody with the function of changing temperature between 270 and 340 K. In normal operation the blackbody is set up at 270 K, and a constant coefficient in a quadratic radiometric calibration equation for each detector is adjusted at that temperature before each Earth observation, but the gain coefficient cannot be adjusted at this time, while it can periodically be updated by long term calibration in which the blackbody is measured at 270, 300, 320, and 340 K. On the other hand the sensor response of all bands (particularly band 12) has been degrading since the launch, and periodical updating of the gain coefficient does not fully follow the degradation, so that the calibration error on level-1 (L1) products is often unacceptable. We therefore have developed a recalibration method which is easily applied to L1 products by a general user. By using this method, the calibration error will mostly be reduced below the level of NEDT.

Keywords: radiometric calibration, degradation, blackbody, at-sensor radiance, level-1 product

1. INTRODUCTION

The Advanced Spaceborne Thermal Emission and Reflection Radiometer (ASTER)[1] is a high-spatial-resolution multispectral imager on the Terra—the first platform of NASA's Earth Observing System (EOS)—launched in December 1999. The ASTER instrument consists of three subsystems divided by the spectral range: the visible and near infrared (VNIR), the short-wave infrared (SWIR), and the thermal infrared (TIR). The TIR subsystem has bands 10 to 14 located at 8.30, 8.65, 9.10, 10.6, and 11.3 μm, respectively, with the spatial resolution of 90 m, and allows us to measure both temperature and spectral emissivity of the land surfaces. The land surface temperature is one of key parameters in the physics of land-surface processes, and used in many environmental studies[2-3]. The land surface spectral emissivity gives useful information particularly to geological studies[4-6], because the spectral emissivity shape in the TIR region changes with the content of silica included in many rocks and soils[7-9].

Since the launch, ASTER/TIR has been working as scheduled, and giving us numerous useful scenes. On the other hand, sensor response to input radiance has continued decreasing since the launch due to degradation[10]: sensor response of band 12 has already been reduced down to 80 % as mentioned later. The first purpose of the present study is to show the degradation status of ASTER/TIR based on onboard calibration data.

Even if a sensor is degrading, it will be able to give accurate at-sensor radiance if radiometric calibration is accurate. In the case of ASTER/TIR, radiometric calibration for at-sensor radiance is not always optimum as mentioned later though the onboard calibrator has been normally working, because updating of radiometric calibration coefficients (RCCs) is not frequent enough in comparison with the degradation rate. In addition, once sensor signals are converted to level-1B (L1B) products (registered at-sensor radiance), recalibration by revising RCCs on a detector-by-detector basis is difficult due to scrambling of detector-by-detector observed lines in geometric resampling. Thus, the second purpose of the present study is to propose a recalibration method applicable to L1B products. This method is easy to use for general users, but radiometric calibration error on L1B products will be remarkably reduced.

---

* tonooka@mx.ibaraki.ac.jp; phone 81 294 38-5292; fax 81 294 38-5158; www.ibaraki.ac.jp
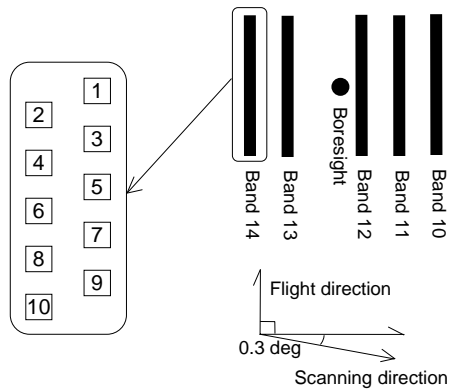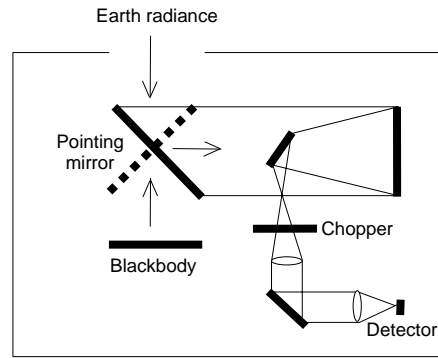
Figure 1: Layout of detectors.

Figure 2: Optics of ASTER/TIR.

2. ASTER/TIR ONBOARD CALIBRATION

ASTER/TIR obtains images by mechanical scanning with 10 HgCdTe PC type detectors aligned along the track for each spectral band (50 detectors in total)[11]. Figure 1 shows the layout of the detectors. As shown in the figure, each detector observes at every 10 lines. Each detector is cooled to 80 K using a mechanical split Stirling cycle cooler.

While each of ASTER/VNIR and SWIR has the function of changing gain, ASTER/TIR does not have and is always operated with normal gain. In ASTER/TIR, uncalibrated digital number (N) is converted to calibrated radiance (R) by a quadratic formula for each detector of each band:

$$R = C_0 + C_1 N + C_2 N^2 \tag{1}$$

where C_0, C_1, and C_2 are RCCs. Each of 50 detectors has a different set of RCCs, and these coefficients will change with condition changes in optics, electronics, and calibration units. Therefore, ASTER/TIR has one honeycombed blackbody with emissivity grater than 0.99 for giving accurate RCCs in the orbit[12]. Figure 2 shows the optics of ASTER/TIR. The sensor can observe the blackbody by rotating the scanning mirror shown in the figure.

Because ASTER/TIR does not have two blackbodies and also cannot observe deep space, it cannot make calibration at two temperature points for each Earth observation. Thus, in normal operation, the blackbody is kept at 270 K and measured before each Earth observation for adjusting C_0 (offset correction). This is called as short term calibration (STC). On the other hand, C_1 and C_2 also will possibly change with condition changes. As for C_1, it is periodically updated by measuring the blackbody at four temperature points of 270, 300, 320, and 340 K. This is called as long term calibration (LTC). In LTC, VNIR and SWIR as well as TIR make calibration using halogen lamps. LTC was executed every 17 days in the early mission period, but the interval has been changed to every 33 days since April 2001 for the reason of keeping the frequency of SWIR pointing below a criterion. As for C_2, it is fixed to a preflight-test value for each detector, because it cannot be so accurately determined from only onboard calibration data. Thus, in each LTC, C_0 and C_1 are calculated under fixed C_2 by the least square method using blackbody observation data at the four temperature points, and C_1 is periodically updated based on LTC results, while C_0 is updated at each Earth observation by STC.

3. ONBOARD CALIBRATION TREND

Figure 3 shows the ratio of C_1 for each detector of each band as a function of the day number (the days since the launch on 18 December 1999), and Table 1 shows actual dates for several day numbers. The ratio of C_1 is defined as
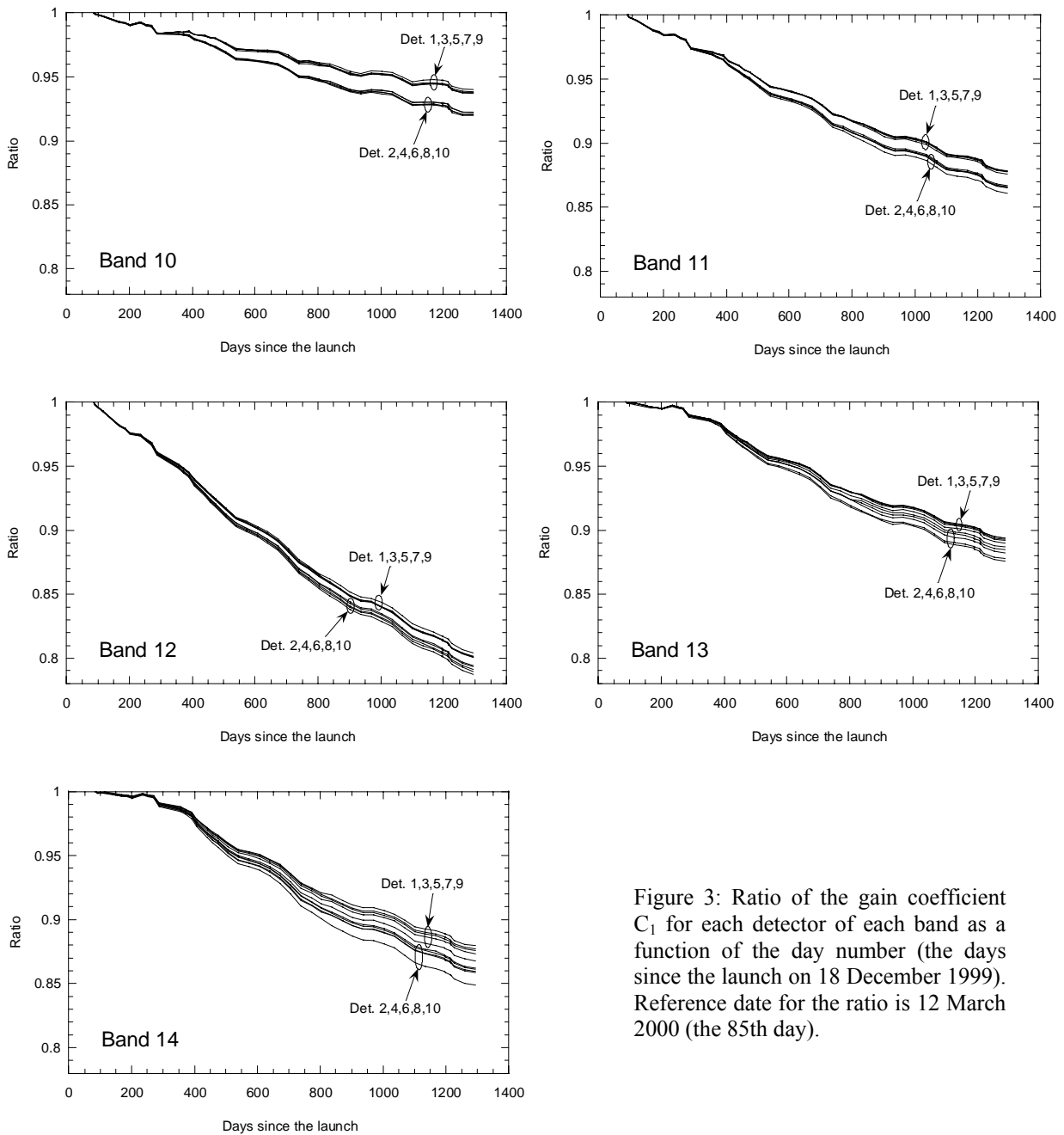
Figure 3: Ratio of the gain coefficient C_1 for each detector of each band as a function of the day number (the days since the launch on 18 December 1999). Reference date for the ratio is 12 March 2000 (the 85th day).

$$\text{Ratio} = C_1^{(\text{ref})} \Big/ C_1^{(\text{target})} \tag{2}$$

where $C_1^{(\text{ref})}$ is C_1 for 12 March 2000 (the 85th day) used as reference, and $C_1^{(\text{target})}$ is C_1 for a target date. These plots indicate the following facts:

(1) The C_1 ratio is decreasing with time for all TIR bands. That is, the sensor response is decreasing with time[10].

(2) The C_1 ratio for band 12 is decreasing most rapidly, and the sensor response of that band has already been reduced down to 80 % from the reference date. Inversely, the C_1 ratio for band 10 is decreasing most slowly.

Table 1: Day number and date.

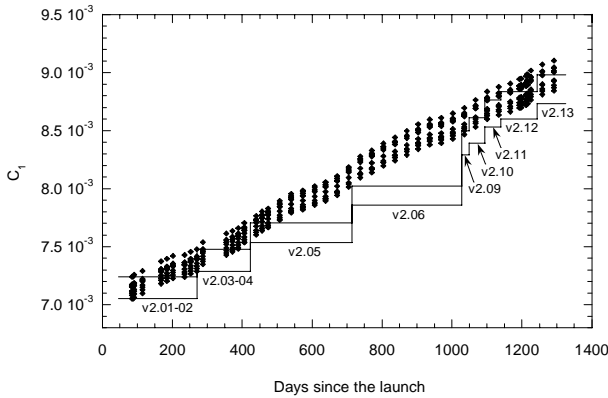| Day number	Date	Day number	Date
0	1999/12/18	800	2002/2/25
200	2000/7/5	1000	2002/9/13
400	2001/1/21	1200	2003/4/1
600	2001/8/9	1400	2003/10/18

Figure 4: Gain coefficient C_1 of band 12 acquired from LTC (shown by dots), and that registered in the RCC database used for L1 processing (shown by solid lines).
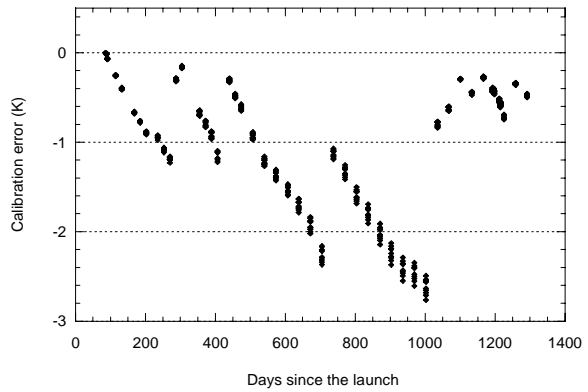
Figure 5: Calibration error (in Kelvin) on L1B products for band 12 at 320 K.

(3) For all bands, odd and even detectors have different behavior in the plots. The sensor response of even detectors is decreasing more rapidly than that of odd detectors.

The cause of (1) is explainable by degradation in optics or electronics. Degradation itself is a common phenomenon in satellite sensors. On the other hand, the causes of (2) and (3) are not fully explainable by degradation in only optics. Therefore, at present we suspect that those have been caused from degradation in electronics, but we need more investigation to clarify these phenomena.

4. USER-BASED RECALIBRATION

4.1 Gain coefficient updating and calibration error

While the offset coefficient C_0 obtained from STC is applied to every level-1 (L1) processing, the gain coefficient C_1 obtained from LTC is not always applied, because L1 processing uses not C_1 obtained from every LTC but C_1 registered to RCC database. The RCC database is updated when calibration errors for 300, 320, and 340 K as of LTC exceed the criteria of 0.5, 0.5, and 1.0 K for 300, 320, and 340 K, respectively, under considering adjustment at 270 K by STC. However this does not mean that the predicted calibration error on L1 products is kept below the criteria, because it takes at least about one month to register C_1 to the RCC database after LTC due to circumstances of international project, and this delay makes the calibration error on L1 products worse than the evaluation as of LTC.

Figure 4 shows the gain coefficient C_1 of band 12 obtained from every LTC and that used for L1 processing. For the former, ten points at each day are corresponding to ten detectors for the band. For the latter, two horizontal lines are

corresponding to the maximum and the minimum of C_1 registered in the RCC database. As shown in the figure, the coefficient is not always optimum at each day, and also the delay in updating the RCC database causes that the updated coefficients have already been old when they begin to be applied to L1 processing.

Figure 5 shows calibration errors on L1 products for band 12 at 320 K as an example. The figure shows that the calibration error is often unacceptable: for example, the error is about -3 K around the 1000th day, while in recent days the calibration error is roughly satisfied with the specified accuracy of less than 1 K for 270-340 K because updating of the RCC database has been improved more frequently.

4.2 Recalibration method for L1B products

As mentioned above, L1 products are not always satisfied with the specified accuracy. In addition, the band dependence of the calibration error will often cause a critical error on higher level processing based on a band-to-band comparison, such as temperature and emissivity separation[13]. Of course, if all products are reprocessed using each optimum RCCs in the future, we have only to wait for final reprocessed products. But at present the project has no plan to reprocess all L1 products, and many products have already been delivered to the user community.

In the case of level-1A (L1A) products (unregistered and uncalibrated radiance), geometric resampling which causes scrambling of detector-by-detector observed lines has not yet been made. In addition, all RCCs applied to next L1B processing are included in L1A HDF metadata, and we can easily replace RCCs on a detector-by-detector basis. Therefore, we will be able to recalibrate accurately and easily for L1A products. On the other hand, in the case of L1B products, we cannot recalibrate on a detector-by-detector basis due to geometric resampling. Moreover we cannot get RCCs from products because they are not included in L1B HDF metadata, and this fact indicates that even if we know the gain coefficient C_1 from the RCC version included in metadata we cannot know the offset coefficient C_0 which is different for each scene. Thus, ideal recalibration should be made to L1A products, but most of L1 products delivered to the user community are not L1A but L1B products. Therefore, we propose a recalibration method applicable to L1B products as mentioned below..

Due to the circumstances of L1B products mentioned above, the method should not have a detector-by-detector basis approach, and also should not need RCCs including C_0. So, first, the followings are assumed.

(1) The onboard calibrator is reliable.

(2) Calibration error at 270 K is negligible due to adjustment by STC.

(3) The effect of the nonlinearity coefficient C_2 is small.

Under these assumptions, we can derive the following formula for recalibrating L1B radiance for each band.

$$R_{recal} = \left(R_{org} - R_{270K}\right)\frac{F(D_{scene})}{F(D_{LTC})} + R_{270K} \qquad (3)$$

where R_{recal} is the recalibrated radiance, R_{org} is the original radiance of L1B, R_{270K} is the radiance at 270 K, D_{scene} is the day number when the scene was observed, D_{LTC} is the day number of LTC giving RCCs applied to the scene, and F is a trend function of C_1 for each band, and the unit of radiance is in W/m^2/sr/μm.

R_{org} is calculated from L1B DN by the following formula.

$$R_{org} = UCC \times \left(N - 1\right) \qquad (4)$$

where UCC is the unit conversion coefficient shown in Table 2. This parameter is constant for each band, and written in L1B HDF metadata. R_{270K} also is constant for each band as shown in Table 3. D_{LTC} is given in Table 4 as a function of the RCC version written in HDF metadata.

The function F(D) was as a cubic equation by regression analysis. That is,

Table 2: Unit conversion coefficient (UCC).

Band	UCC
10	0.006882
11	0.006780
12	0.006590
13	0.005693
14	0.005225

Table 3: Radiance at 270 K.

Band	R_{270K}
10	4.915
11	5.191
12	5.469
13	5.876
14	5.841

Table 4: LTC date and its day number for each RCC version.

RCC version	LTC date	Day number
2.01, 2.02	2000/3/12	85
2.03, 2.04	2000/9/13	270
2.05	2001/1/27	406
2.06	2001/8/16	607
2.09	2002/5/7	871
2.10	2002/8/13	969
2.11	2002/11/20	1068
2.12	2002/12/23	1101
2.13	2003/4/17	1216

Note: Versions 2.07 and 2.08 are not used for normal level 1 processing.

Table5: Coefficients of the function F for three periods. The coefficients for the third period were derived by extrapolation, and will be updated in the future.

Start day	End day	Coefficient	Band 10	Band 11	Band 12	Band 13	Band 14
85	650	a_0	7.6940E-03	7.3299E-03	7.1010E-03	6.3132E-03	5.8652E-03
		a_1	4.3350E-07	3.7962E-07	4.0530E-07	-1.0811E-06	-1.3399E-06
		a_2	-1.2387E-10	1.3728E-09	3.1407E-09	4.3583E-09	5.0933E-09
		a_3	3.6673E-13	-9.1356E-13	-2.4717E-12	-3.1286E-12	-3.6291E-12
650	1300	a_0	6.0424E-03	5.2127E-03	4.4169E-03	4.2338E-03	3.5926E-03
		a_1	5.7039E-06	7.5693E-06	9.8127E-06	6.7513E-06	7.2686E-06
		a_2	-5.2967E-09	-6.7810E-09	-8.4413E-09	-6.1424E-09	-6.5348E-09
		a_3	1.7348E-12	2.2195E-12	2.7731E-12	2.0135E-12	2.1351E-12
1300	—	a_0	7.6679E-03	7.2505E-03	6.9701E-03	6.1247E-03	5.6444E-03
		a_1	5.7009E-07	1.0765E-06	1.6884E-06	7.1791E-07	7.5124E-07
		a_2	-6.0573E-11	-1.1530E-10	-1.0797E-10	-2.4168E-12	4.4184E-11
		a_3	0	0	0	0	0

$$F(D) = a_0 + a_1 D + a_2 D^2 + a_3 D^3 \qquad (5)$$

where a_0, a_1, a_2, a_3 are regression coefficients, and D is the day number. For better accuracy, we determined these coefficients using all LTC data (50 sets acquired in 85-1292 day) for each of three periods: the 85-650 day, the 650-1300 day, and the 1300 and later day. Table 5 shows all coefficients determined for each period, and Figure 6 shows plots of C_1 and the function F for each band. The third period is the future at present, so the equations were determined by extrapolation as a quadratic form for reducing an extrapolation error. In the future, the coefficients for that period will be updated.
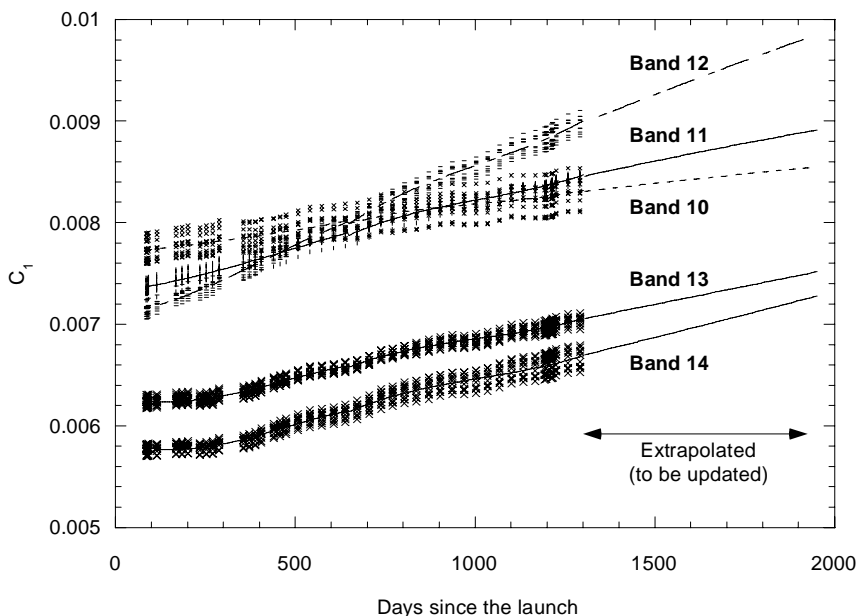
Figure 6: Plots of the gain coefficient C_1 (shown as dots) and the trend function F (shown as a curve) for five bands.

4.3 Validation

The main error factors for the proposed method are as follows:

(1) Detector-to-detector deviation

(2) Form of the function

(3) Nonlinearity of the radiometric calibration formula

To evaluate the accuracy of the proposed method, we calculated calibration errors for original and recalibrated radiances using all LTC data. Figure 7, 8, and 9 show the results for 300, 320, and 340 K, respectively. As shown in the figures, the original radiance often has a critical calibration error which is larger for higher temperature and for more degrading band. In the most critical case (band 12 at 340 K around the 1000th day), the error has reached to -3.5 K. Incidentally, the error on the original radiance in recent days is usually kept below a lower level because updating of RCCs has come to be executed more frequently, as mentioned before. On the other hand, the figures show that the proposed method works well, and the recalibrated radiance in most cases is comparable to the level of NEDT (noise equivalent delta temperature, 0.3 K for ASTER/TIR). The worst is the case of band 14 at 340 K, but its error is 0.5 K at most.

5. CONCLUTIONS

ASTER/TIR has been degrading since the launch. The first feature of its rate is to be different among bands: band 12 is degrading most rapidly and the sensor response has already reduced down to 80 % since the launch, while band 10 is degrading most slowly. The second feature is to be different between odd and even detectors for each band: the degradation of even detectors is more rapidly than that of odd detectors. The causes for these have not been clarified yet and we need more investigation, while at present we suspect that the causes are condition changes in electronics.

On the other hand, updating of RCCs applied to L1 processing is not fully following the degradation, and the calibration error is often unacceptable. In recent days the calibration accuracy has come to be roughly kept within the specification

by more frequent updating, but many L1B products have been already delivered to the user community. We therefore have developed a recalibration method which can easily recalibrate L1B products. The proposed method is affected by such error factors as detector-to-detector deviation, straying from the trend function, and nonlinearity, but can remarkably reduce the calibration error on original radiance, and the predicted error is roughly kept below the level of NEDT. Though we showed the coefficients of the function F for three periods in this paper, the coefficients for the third period were derived by extrapolation. We will update and present them with the latest D_{LTC} on some Web sites of the ASTER project.

ACKNOWLEDGMENTS

REFERENCES

1. Yamaguchi, Y., A. B. Kahle, H. Tsu, T. Kawakami, and M. Pniel, "Overview of Advanced Spaceborne Thermal Emission and Reflectance Radiometer (ASTER)", *IEEE Trans. Geosci. Remote Sens.*, **36**, pp. 1062-1071, 1998.
2. Schmugge, T. J., W. P. Kustas, and K. S. Humes, "Monitoring land surface fluxes using ASTER observations", *IEEE Trans. Geosci. Remote Sens.*, **36**, pp. 1421-1430, 1998.
3. Watson, K., "Regional thermal-inertia mapping from an experimental satellite", *Geophys.*, **47**, pp. 1681-1687, 1982.
4. Kahle, A. B., "Surface emittance, temperature, and thermal inertia derived from Thermal Infrared Multispectral Scanner (TIMS) data for Death Valley, California", *Geophys.*, **52**, pp. 858-874, 1987.
5. Crisp, J., A. B. Kahle, E. A. Abbott, "Thermal infrared spectral character of Hawaiian basaltic glasses", *J. Geophys. Res.,* **95B**, pp. 21657-21669, 1990.
6. Abrams, M., E. Abbott, A. Kahle, "Combined use of visible, reflected infrared, and thermal infrared images for mapping Hawaiian lava flows", *J. Geophys. Res.*, **96B**, pp. 475-484, 1991.
7. Lyon, R. J. P., "Analysis of rocks by spectral infrared emission (8 to 25 microns)", *Econ. Geol.*, **60**, pp. 715-736, 1965.
8. Salisbury, J. W., L. S. Walter, and D. D'Aria, *Midinfrared (2.5 to 13.5 μm) spectra of igneous rocks*, USGS Open File Report 88-686, US Geological Survey, Reston, VA, 1988.
9. Salisbury, J. W., and D. M. D'Aria, "Emissivity of terrestrial materials in the 8-14 μm atmospheric window", *Remote Sens. Environ.,* **42**, pp. 83-106, 1992.
10. Sakuma, F., F., A, Ono, M. Kudoh, H. Inada, S. Akagi, H. Ohmae, "ASTER on-board calibration status", *Proc. SPIE*, **4881**, pp. 407-418, 2002.
11. Fujisada, H., H. Sakuma, A. Ono, and M. Kudoh, "Design and preflight performance of ASTER instrument protoflight model", *IEEE Trans. Geosci. Remote Sens.*, **36**, pp. 1152-1160, 1998.
12. Ono, A., F. Sakuma, K. Arai, Y. Yamaguchi, H. Fujisada, P. Slater, K. Thome, F. Palluconi and H. Kieffer, "Preflight and In-Flight Calibration Plan for ASTER", *J. Atmos. Oceanic Techn.*, **13**, pp. 321-335, 1996.
13. Gillespie, A., S. Rokugawa, T. Matsunaga, J. S. Cothern, S. Hook, and A. B. Kahle, "A temperature and emissivity separation algorithm for Advanced Spaceborne Thermal Emission and Reflection Radiometer (ASTER) Images", *IEEE Trans. Geosci. Remote Sens.*, **36**, pp. 1113-1126, 1998.
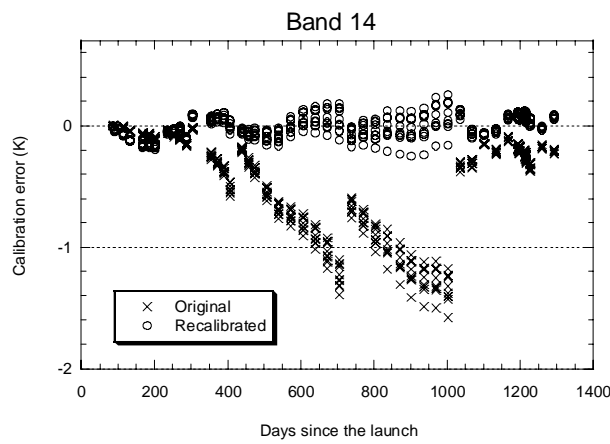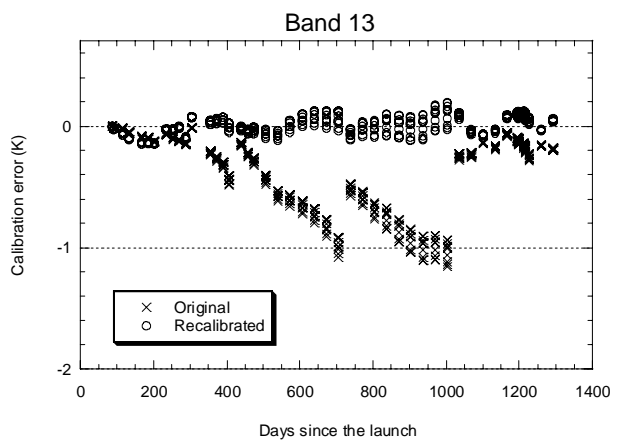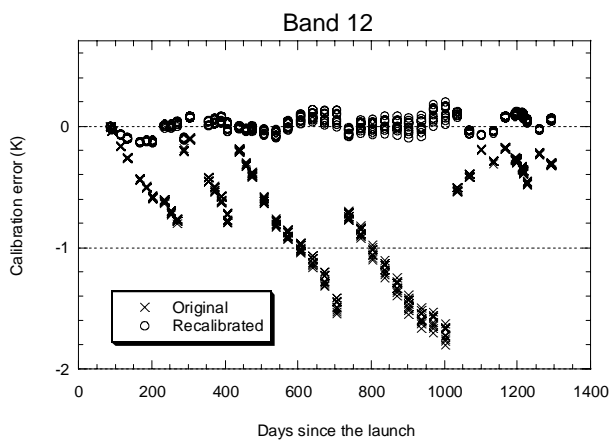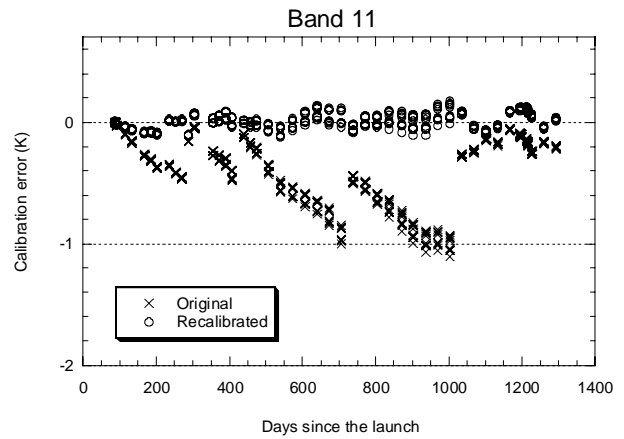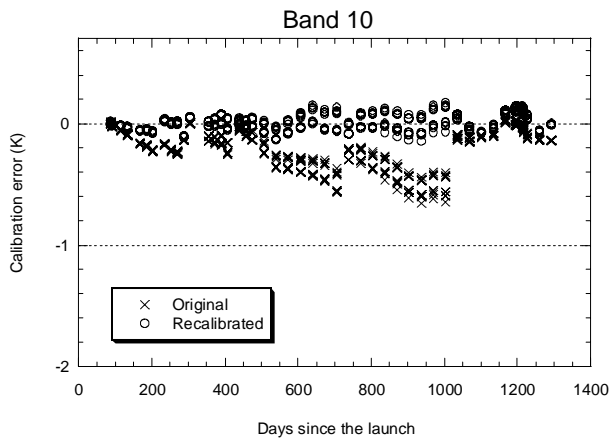
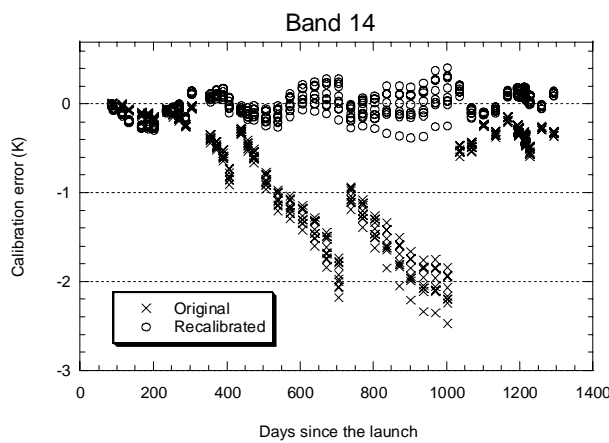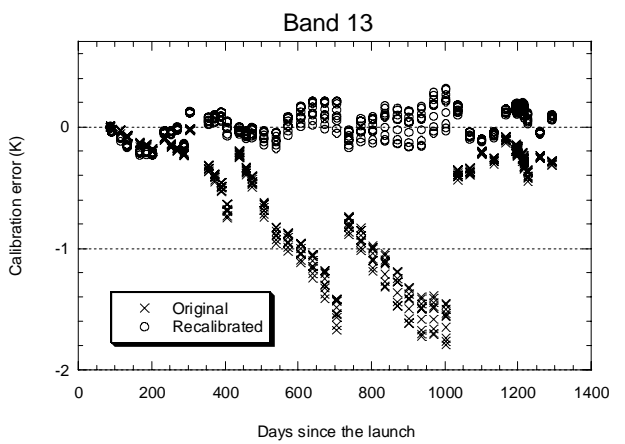Figure 7: Comparison of calibration errors (in Kelvin) at 300 K between original radiance and recalibrated radiance.
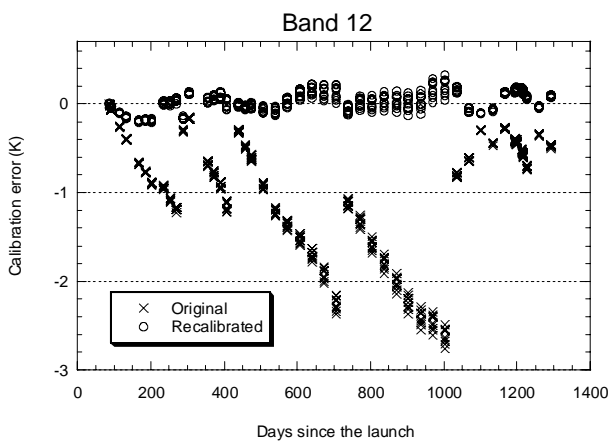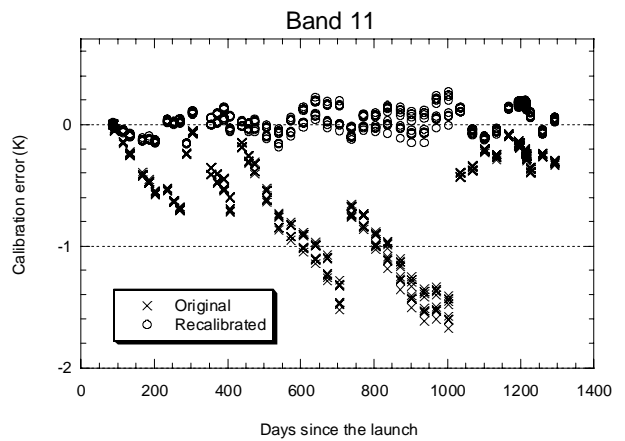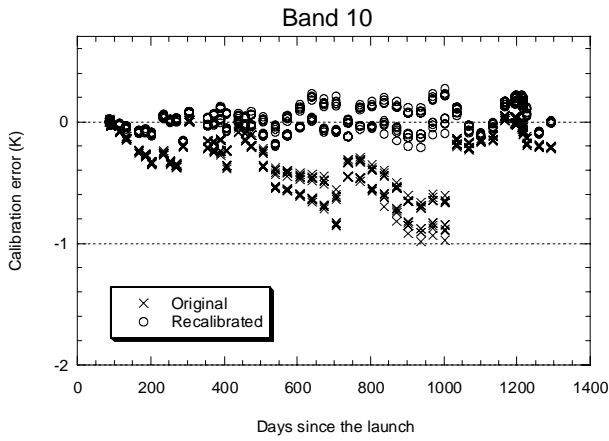
Figure 8: Comparison of calibration errors (in Kelvin) at 320 K between original radiance and recalibrated radiance.
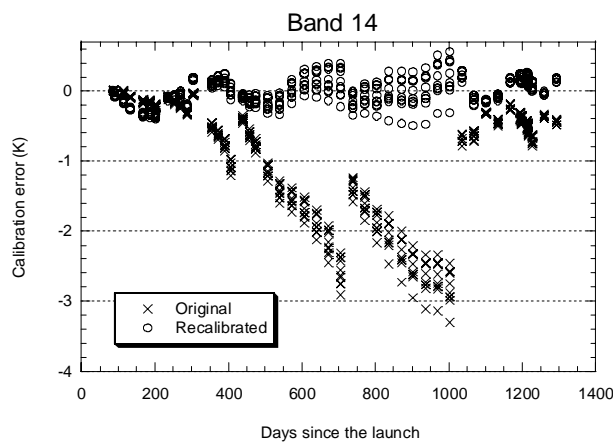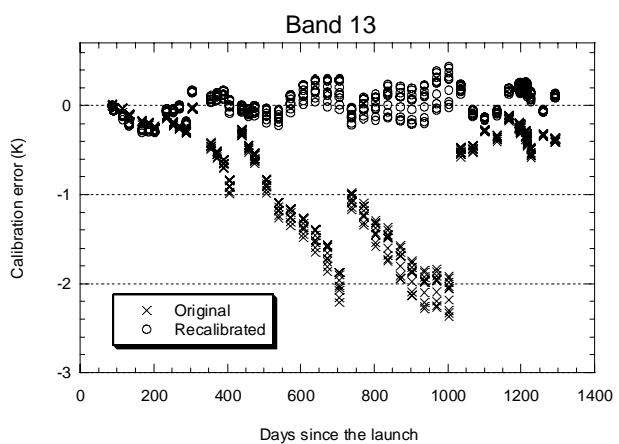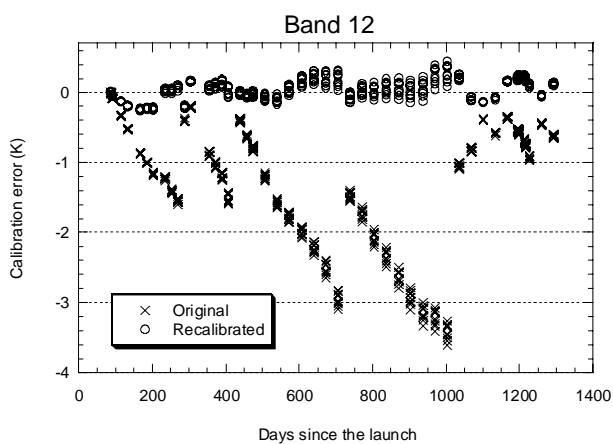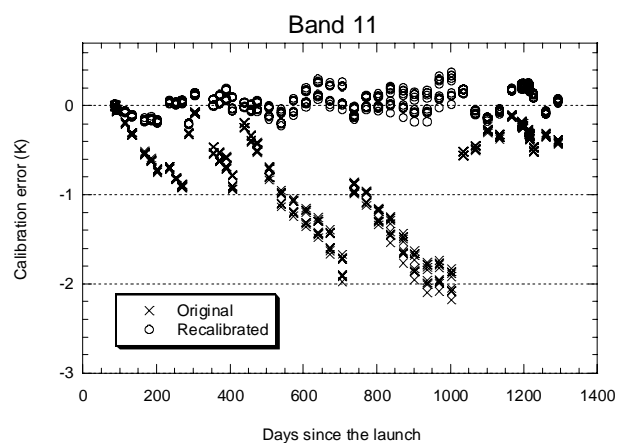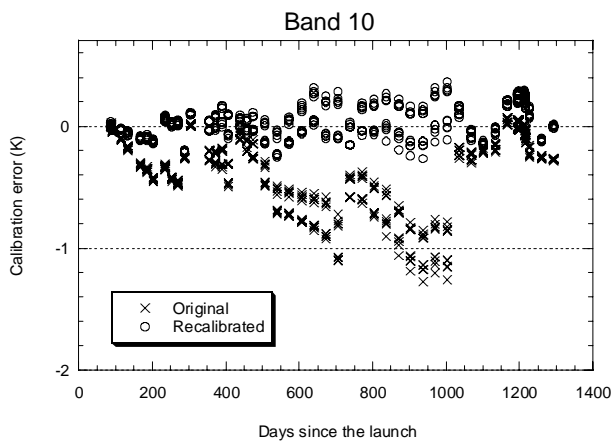
Figure 9: Comparison of calibration errors (in Kevin) at 340 K between original radiance and recalibrated radiance.